ACS SENSORS

Article

Cite This: ACS Sens. XXXX, XXX, XXX−XXX

pubs.acs.org/acssensors

Transcutaneous Blood VOC Imaging System (Skin-Gas Cam) with Real-Time Bio-Fluorometric Device on Rounded Skin Surface

Kenta Iitani,[†,‡,§] Koji Toma,[§] Takahiro Arakawa,[§] and Kohji Mitsubayashi*[,§]

[†]Japan Society for the Promotion of Science, 5-3-1 Kojimachi, Chiyoda-ku, Tokyo 102-0083, Japan

[‡]Department of Life Science and Medical Bioscience, Graduate School of Advanced Science and Engineering, Waseda University (TWIns), 2-2 Wakamatsu-cho, Shinjuku-ku, Tokyo 162-8480, Japan

[§]Department of Biomedical Devices and Instrumentation, Institute of Biomaterials and Bioengineering, Tokyo Medical and Dental University (TMDU), 2-3-10 Kanda-Surugadai, Chiyoda-ku, Tokyo 101-0062, Japan

Supporting Information

ABSTRACT: A skin-gas cam that allows continuous imaging of transcutaneous blood volatile organic compounds (VOCs) emanated from human skin was developed. The skin-gas cam is able to reveal the relationship between the local skin conditions and transcutaneous blood VOCs in the field of volatile metabolomics (volatolomics). A ring-type ultraviolet (UV) light-emitting diode was mounted around a camera lens as an excitation light source, which enabled the simultaneous excitation and imaging of fluorescence. A nicotinamide adenine dinucleotide (NAD)-dependent alcohol dehydrogenase (ADH) was used to detect ethanol as a model sample. When gaseous ethanol was applied to an ADH-immobilized mesh that was wetted with an oxidized NAD solution placed in front of the camera, a reduced form of NAD (NADH) was produced through an ADH-mediated reaction. NADH emits fluorescence by UV excitation, and thus, the concentration distribution of ethanol was visualized by measuring the distribution of the fluorescence light intensity from NADH on the ADH-immobilized mesh surface. In this study, a new gas application method that mimicked the release mechanism of transcutaneous gas for quantification of the transcutaneous gas concentration was evaluated. Also, spatiotemporal changes of transcutaneous ethanol for various body parts were measured. As a result, we revealed a relationship between local skin conditions and VOCs that could not be observed previously. In particular, we demonstrated the facile measurement of transdermal gases from around the ear where capillaries are densely distributed below a thin stratum corneum.

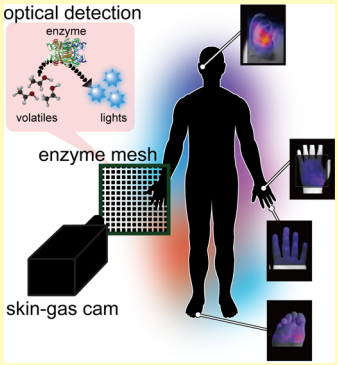

KEYWORDS: *transcutaneous volatile, enzyme, biosensor, fluorescence, volatolomics, spatiotemporal imaging*

Volatile organic compounds (VOCs) that derived from human are used to assess health conditions. Recently, volatile metabolomics, so-called volatolomics,[1] has been applied in medical research, in addition to disease screening. Dating back to ancient Greece, disciples of Hippocrates made use of VOCs released from humans as an aid in disease diagnosis.[2] Since VOCs in exhaled breath and transcutaneous gas reflect the VOCs present in circulating blood, investigation of these gases allows us to realize metabolic disorders, genetic disorders, and oncogenesis.[3,4]

VOCs are commonly analyzed in laboratories using a large-scale system such as gas chromatography (GC)−mass spectrometry (MS),[5] proton transfer reaction−MS,[6] selected-ion-flow tube−MS,[7] and solid-phase-microextraction−MS.[8] Although these methods have high sensitivity and high selectivity, they are unsuitable for smaller-scale analysis because of the price and size of the instruments, the time required for analysis, and the complexity of their operation.

Chemical sensors that have been functionalized using various materials such as metal oxides and organic or inorganic materials can be fabricated compactly and inexpensively. Therefore, they are promising candidates for the monitoring of VOCs in a nonlaboratory environment. For instance, a system for detecting VOCs has been developed by mounting a small gas sensor in a near-field communication tag and reading out the sensor output with a smartphone.[9] Such chemical sensors, however, have difficulties in achieving both high selectivity and sensitivity because they measure changes in physical quantities, such as electrical resistance and mass, which is caused by the adsorption of VOCs onto the functional materials.[10] When measuring VOCs in biological samples such as exhaled breath and transcutaneous gas for medical purposes, both high selectivity and sensitivity are required since breath and transcutaneous gas are complicated mixtures containing parts-per-trillion (ppt) to parts-per-million (ppm) extent of VOCs.[11]

In recent years, we have conducted research studies focusing on transcutaneous VOCs as substances that may be used to monitor human health in comparison to breath VOCs. Breath

Received: August 26, 2019
Accepted: November 28, 2019

DOI: 10.1021/acssensors.9b01658
ACS Sens. XXXX, XXX, XXX−XXX

VOCs are easy to measure because the concentration range of VOCs in breath is at a parts-per-billion (ppb) to ppm level. However, it is difficult to use these VOCs for long-term monitoring as it is necessary to use a special mask when the continuous measurement of a change in concentration is required. This mask is required to collect only end-tidal air,[12,13] but it increases the burden on the subject. On the other hand, as transcutaneous gas is released continuously, it is more appropriate than breath for the continuous monitoring of a changing VOC concentration over time.[14] However, the drawback of the conventional transcutaneous gas measurement method is that the resolution of the measurement of time is reduced due to the gas condensation process.[15−17] In addition, transcutaneous gas has a unique characteristic in which the entire skin surface area of 1.6 m^2 may release VOCs. The number of stratum corneum layers,[18] distribution of capillary vessels, and activity of secretory glands[19] differ depending on the part of the skin; hence, it has been reported that the concentration of transcutaneous VOCs varies with the different body parts.[20,21] Therefore, spatial information, such as the concentration distribution, must be taken into account, in addition to temporal information such as the change in concentration of VOCs over time.

Previously, we have developed a highly sensitive bio-fluorometric gas sensor "bio-sniffer" based on an enzymatic reaction and measured the concentration of transcutaneous ethanol (EtOH) after drinking in real-time.[22] We are also developing a gas-imaging system, the "Sniff-cam", that extends the detection principle of the bio-sniffer to the measurement of the spatiotemporal distribution of VOCs.[23,24] However, the conventional Sniff-cam had three issues: (I) transmissive UV light was blocked by the body during the application of transcutaneous gas because of the optical design; (II) the quantitative imaging of transcutaneous gas was not achieved since the concentration calibration method of the system was not consistent with the release mechanism of the transcutaneous gas; (III) the complex irregularities of the surface of the human body were not considered. Because of these problems, the real-time and quantifiable spatiotemporal imaging of transcutaneous gas has not yet been achieved.

In this study, we first developed a "skin-gas cam" that is a specialized system for real-time transcutaneous gas-imaging and a gas application method mimicking the release mechanism of transcutaneous gas. Then, we demonstrated the potential of the developed system by measuring transcutaneous EtOH and acetaldehyde (AcH) emitted from a human subject who had consumed alcohol.

EXPERIMENTAL SECTION

Gas-Imaging System for Blood VOCs Derived from Human Body. An enzymatic reaction of alcohol dehydrogenase (ADH, EC 1.1.1.1) that has a substrate specificity toward EtOH was utilized for the selective imaging of EtOH. The ADH catalyzed the oxidation of EtOH to AcH and the reduction of the oxidized form of nicotinamide adenine dinucleotide (NAD^+) to the reduced form of nicotinamide adenine dinucleotide (NADH) under alkaline conditions (Figure 1a). NADH that was produced in the enzymatic reaction of ADH shows an absorbance peak at 340 nm and emits fluorescent light at a 490 nm wavelength when excited with UV light. The intensity of the fluorescent light emitted from NADH depends on its concentration, which is produced by the ADH reaction. Regarding the fact that NADH concentration is correlated with the concentration of EtOH, the concentration of EtOH can be quantified by measuring the intensity of the fluorescent light emitted from NADH. To measure

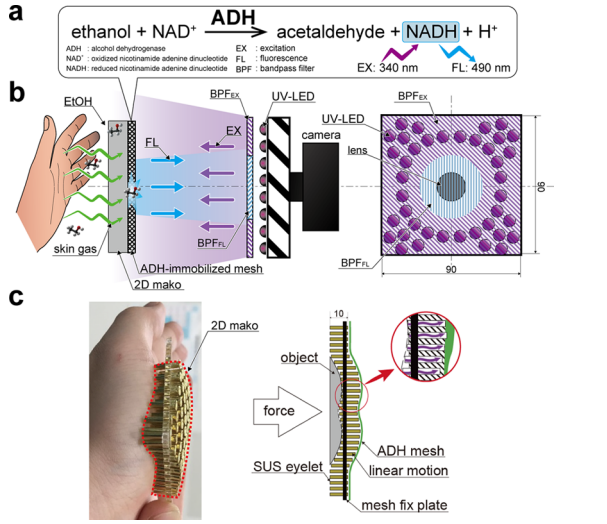

Figure 1. (a) Detection principle of the EtOH based on the ADH-mediated catalytic reaction. (b) Schematic diagram of the skin-gas cam. (c) Working mechanism of two-dimensional (2D) Mako.

the spatial distribution of the EtOH concentration in the gaseous phase, we used a 90 mm × 90 mm ADH-immobilized mesh. The spatiotemporal change in the EtOH concentration can be measured by the distribution of the fluorescence intensity of NADH. The preparation of the mesh is described in the next section.

Figure 1b illustrates the conceptual diagram of the skin-gas cam. This system was mainly composed of a commercially available camera (ILCE-7s, Sony, Japan), two bandpass filters (BPF) for excitation light (BPF_{EX}, λ = 340 ± 42.5 nm; HOYA, Japan) and fluorescence light (BPF_{FL}, λ = 492 ± 10 nm; Edmund), an excitation light source with UV light-emitting diodes (LEDs) (340X40L8SB, custom-made, Dowa, Japan), the ADH-immobilized mesh, and a 2D pipe array (2D Mako). This system allowed continuous real-time imaging of transcutaneous EtOH via the excitation and fluorescence imaging of NADH produced in the ADH-immobilized mesh from the same direction, which was impossible when using the previous Sniff-cam. The excitation light source structure is also shown in Figure 1b. Forty ultraviolet light-emitting diode (UV-LEDs) (λ = 340 ± 5 nm; UF-4VG-2H004, Dowa, Japan) with different radii were arranged concentrically. The excitation light source was integrated with the camera by inserting a lens into a through-hole of the excitation light. The square BPF_{EX} and circular BPF_{FL} were placed on the same plane. The BPF_{EX} was custom-made with dimensions of 100 mm × 100 mm, a thickness of 2.5 mm, and a through-hole 75 mm in diameter at the center. The excitation light source was connected to the control box and the DC-stabilized power supply (KX-100X, Takasago, Japan). The camera was controlled by the computer, and fluorescence images captured by the camera were sent to the computer via a video encoder (Intensity Shuttle, Blackmagic Design, Australia) to observe the real-time change in the fluorescence. The fluorescence distribution was captured as a red-green-blue (RGB) color image with a size of 1920 pixels × 1080 pixels.

Besides, we used the 2D Mako to equalize the distance between the complex surface shape of the body and the ADH-immobilized mesh according to the irregularities of the skin surface. Since a rigid honeycomb plate was used as a spacer between the skin surface and the ADH-immobilized mesh in the previous study, the time required to reach the ADH-immobilized mesh may change even when the VOCs are released simultaneously from the skin surface (see Figure S1). Therefore, evaluation of the spatiotemporal changes of the VOC concentration in transcutaneous gas was difficult. In the method using a 2D Mako, each pipe that could slide back and forth through a hole individually in an acrylic plate was used to deform the ADH-immobilized mesh that was pasted on the surface of the 2D Mako (see Figure 1c). Thus, the distance between the skin surface and the

DOI: 10.1021/acssensors.9b01658
ACS Sens. XXXX, XXX, XXX−XXX

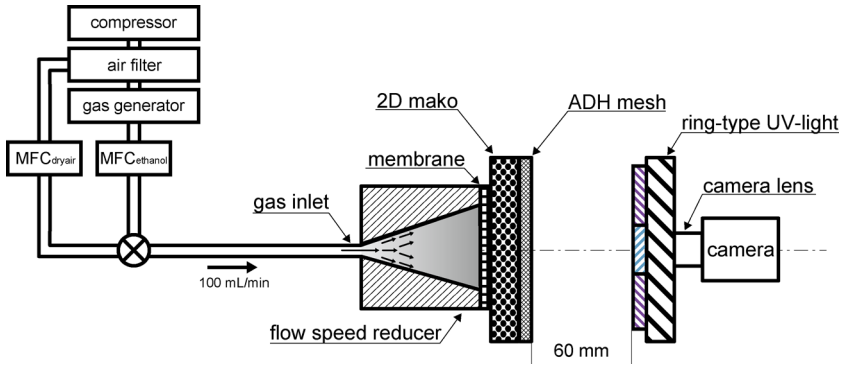

Figure 2. Experimental setup for the standard gaseous EtOH imaging to evaluate the dynamic range of the developed Sniff-cam.

ADH-immobilized mesh could be kept at the pipe length, 10 mm, at any position of the measurement area when the uneven surface of the body was in contact with the 2D Mako.

Preparation of an ADH-Immobilized Mesh. ADH (0.365 mg, 60 units/cm^2, 369 units/mg solid, from *Saccharomyces cerevisiae*; A7011, Sigma-Aldrich) and 0.56 mg of bovine serum albumin (BSA; 306-13383, Wako, Japan) were dissolved in 112.5 μL phosphate buffer solution (PB; 50 μL/cm^2 at pH 8.0, 0.1 M) to prepare the enzyme solution. Next, the enzyme solution was spread homogeneously on a 15 mm × 15 mm square of a cotton mesh (ISBN# 4987379020036; Ohki Healthcare Holdings, Japan), and then the cotton mesh that absorbed the enzyme solution was stored in a refrigerator for 1 h. Next, 18 μL of glutaraldehyde (GA; 8 μL/cm^2) solution that was prepared by a 10-fold dilution of a stock solution of GA (25%; 079-00533, Wako, Japan) with PB (at pH 7.0, 0.1 M) was applied dropwise onto the enzyme-absorbed cotton mesh. The cotton mesh was then stored in the refrigerator for 1.5 h to allow crosslinking between ADH and BSA. Finally, the excess ADH on the cotton mesh was rinsed off using 80 μL/cm^2 of PB (at pH 8.0, 0.1 M).

Evaluation of the 2D Uniformity of Excitation Light Intensity. We evaluated the uniformity of the excitation light intensity at a 340 nm wavelength emitted from the custom-made excitation light source. Irradiating uniform intensity of excitation light onto a 2D surface is essential to measure the concentration distribution of EtOH appropriately because the fluorescence light from NADH at a 490 nm wavelength varies with the intensity of the excitation light.

The experimental setup for the evaluation of the 2D uniformity of the excitation light intensity is shown in Figure S2. The 2D distribution of the excitation light intensity was captured with the camera by utilizing a white paper (Super white+, Askul, Japan) that emitted fluorescence at around 490 nm resulting from the fluorescent whitening agent irradiated with the excitation light. The distance between the white paper and the excitation light, L, was varied at 0, 50, 60, 70, 80, 90, 100, 150, 200, and 300 mm to find the optimal distance. The uniformity and intensity of the excitation light at each distance were evaluated using the standard deviation and mean of the fluorescence, which was calculated using ImageJ[25] with the Python script.

Development of a Gas Application Device that Enables 2D Gas Application. Previously, to evaluate the quantitative characteristics and response to standard gaseous samples of a known concentration, we applied a standard gaseous sample at a flow rate of 100 mL/min to the center of an ADH-immobilized mesh through a gas injector constructed with a glass Pasteur pipette, as shown in Figure S3a. The previous calibration method was not as accurate as of the new method because of the fundamental differences between the emission mechanism of transcutaneous gas that is released through the dermis and epidermis. Therefore, we developed a new gas application device that enables the application of gaseous samples to a 2D surface at a low flow rate. Figure S3b displays the concept of the new gas application device that was constructed with a funnel-like structure as a gas speed reducer and a porous membrane as a gas diffusion membrane.

Figure S4a,b shows dimensions of the funnel-like speed reducer and the overview of the new gas application device. The gas application device had a structure that can be disassembled and the gas diffusion membrane was fixed by a silicon O-ring so that it can be easily replaced. Subsequently, experiments using various kinds of gas diffusion membranes were performed to find a suitable one. The specifications of the porous membranes used for comparison are shown in Table S1. The material of the porous membrane was chosen based on its antiadsorption characteristics of chemicals.

In the experiment, the gas application device with a porous membrane was placed in a sample bag and sealed. Gaseous EtOH (200 ppm) was then introduced into the gas application device to evaluate the recovery rate. Subsequently, the concentration of gaseous EtOH in the sample bag that diffused via the porous membrane was measured by a gas detection tube (#112L, Gastec, Japan).

Next, we evaluated the uniformity of the concentration distribution of EtOH emitted from the developed gas injection device by measuring the fluorescence distribution when 5 ppm of gaseous EtOH was applied to an ADH-immobilized mesh. In this experiment, 10 mM of an NAD$^+$ solution (in Tris−HCl buffer at pH 9.0, 0.1 M, 80 μL) was applied dropwise onto the ADH-immobilized mesh. The gas application method consisted of (I) recording simultaneously in 2 min with dry air application, (II) switching to 5 ppm of gaseous EtOH and applying for 2 min, and (III) changing to dry air and applying for 3 min. The recorded fluorescence images were analyzed by ImageJ with a Python script to evaluate the fluorescence intensity distribution.

Evaluation of the Dynamic Range of the Developed System. An experimental setup for the evaluation of quantitative characteristics using a uniform 2D-surface concentration with a low flow rate and standard gas application method is shown in Figure 2. This experiment utilized a 2D Mako as well as spatiotemporal imaging of the transcutaneous gas and a gas injection device placed on the backside of the 2D Mako, whereas a 90 mm × 90 mm ADH-immobilized mesh sample with 2280 μL of NAD$^+$ solution (10 mM in Tris−HCl at pH 9.0, 0.1 M) was attached to the front of the 2D Mako. The same gas application method used to test the uniformity of the concentration distribution of EtOH from the developed gas application device was used. The recorded fluorescence images were processed by the bicolor method,[26] then the differential analysis method was used to calculate the time course of fluorescence intensity and the changing rate of fluorescence. Finally, the concentration dependence of the system on the gaseous EtOH was evaluated.

Spatiotemporal Imaging of Gaseous EtOH Emitted from Different Body Parts. Experiments involving human samples were submitted to the Tokyo Medical and Dental University Ethics Committee and performed after approval (approval number M2018-160). We explained the purpose and method of the experiments to the subjects who agreed to cooperate with the study and then measured the body temperature, blood pressure, and heart rate to find healthy adult subjects. Subsequently, an EtOH patch test,[27] a simple test for checking a gene polymorphism of aldehyde dehydrogenase 2

DOI: 10.1021/acssensors.9b01658
ACS Sens. XXXX, XXX, XXX−XXX

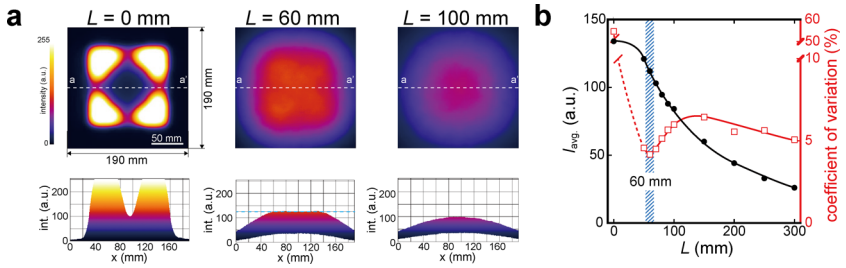

Figure 3. (a) Distribution of the excitation light intensity with different distances, L (0, 60, and 100 mm) between the ring-type UV-LED light and the excitation target. (b) The relationship between L and the average intensity of the excitation light, I_{avg} (●), and the CV of the excitation intensity (□) over an area of 90 mm × 90 mm on the excitation target.

a

application type		gas blowing	gas diffusion			
membrane	material	N/A	polytetrafluoroethylene			glass
	pore size	N/A	0.2 μm	1.0 μm	5.0 μm	300.0 μm
FL distribution						
recovery rate (%)		100	75	95	100	100

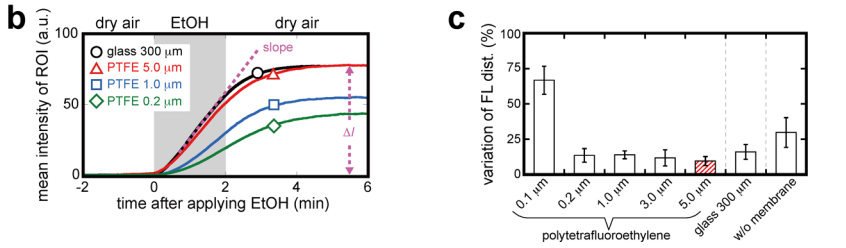

Figure 4. (a) Summary of the typical results of the fluorescence distribution and EtOH concentration recovery rate that was obtained using different types of porous membranes as the gas diffusion membrane. (b) Time course of mean fluorescence intensity with the application of gaseous EtOH via a developed gas injection device with different porous membranes (○ glass mesh; Δ PTFE with 5 μm of pore diameter; □ PTFE with 1 μm of pore diameter; ◇ PTFE with 0.2 μm of pore diameter). (c) Comparison of the variation in the fluorescence intensity distribution that is shown in (b).

(ALDH2), was performed after the subjects finished filling out a questionnaire about their physical conditions on the day of evaluation. In the patch test, a plaster patch containing EtOH (Cat# 14033-00; Kanto Kagaku, Japan) was placed on the inside of the forearm, and the EtOH patch was removed after 7 min. It is possible to observe ALDH2 gene polymorphism of the subject by observing a color change at the skin at 10 min after the removal of the patch. We classified whether the subject had flushing of the skin 17 min after attaching the alcohol patch to a group of low-activity ALDH2 participants (ALDH2[−]). Otherwise, the subject was classified as having high ALDH2 activity (ALDH2[+]). Note that when flushing of the skin was observed 7 min after placing the alcohol patch on the arm of a subject, it was judged that the risk due to alcohol drinking was high, and subsequent experiments were not performed on those subjects. In this experiment, distilled liquor (EtOH of 25%) was taken orally over 15 min. The amount of alcohol was fixed to 0.4 g of EtOH per 1 kg of body weight of the subject to equalize the consumption rate of EtOH in alcohol metabolism in each subject. A 90 mm × 90 mm square of the ADH-immobilized mesh moistened with 2280 μL of NAD^+ solution (10 mM in Tris−HCl at pH 9.0, 0.1 M) was attached to the surface of the 2D Mako. Then, the target body part was pressed from the opposite side of the 2D Mako to fit the shape of the ADH-immobilized mesh to the body surface. Fluorescence images were processed by the bicolor method, and the differential analysis method was used to calculate the temporal change of the changing fluorescence rate to quantify the transcutaneous EtOH concentration based on the calibration curve shown in eq 1.

Spatiotemporal Imaging of EtOH and AcH Emitted Around the Ear. Ears are less prone to sweating than other body parts and also have a high density of capillary blood vessels under a thin stratum corneum, thus allowing the release of VOCs contained in blood via transcutaneous gas. Therefore, they were considered as a suitable site for monitoring blood VOCs via transcutaneous gas. We evaluated the spatiotemporal changes in transcutaneous EtOH and AcH concentration around the ear based on a reversible reaction of ADH.[28,29] In the experiment, an ear of the healthy subject was brought into contact with the 2D Mako such that the ADH-immobilized mesh was exposed to transcutaneous gas after the patient had consumed alcohol. Since the simultaneous imaging of EtOH and AcH was not possible with the current system, the spatiotemporal imaging of the transcutaneous AcH was performed 3 days after the experiment for the spatiotemporal imaging of EtOH for each subject to avoid the influence of residual EtOH. We used two 90 mm × 90 mm squares of the ADH-immobilized mesh for spatiotemporal imaging, one with 2280 μL of the NAD^+ solution (10 mM in Tris−HCl at pH 9.0, 0.1 M) for EtOH and another with 2280 μL of NADH solution (0.5 mM, in Tris−HCl at pH 6.5, 0.1 M) for AcH.

RESULTS AND DISCUSSION

Two-Dimensional Uniformity of the Excitation Light Intensity. Figure 3a shows the distribution of the excitation light intensity when L, which is defined as the distance between the excitation light source and the target, was 0, 60, and 100 mm. Additionally, Figure 3b shows the relationship between the L and the excitation light intensity or 2D uniformity of the light. The excitation light intensity showed a maximum value when the distance L was 50 mm, and it then

DOI: 10.1021/acssensors.9b01658
ACS Sens. XXXX, XXX, XXX−XXX

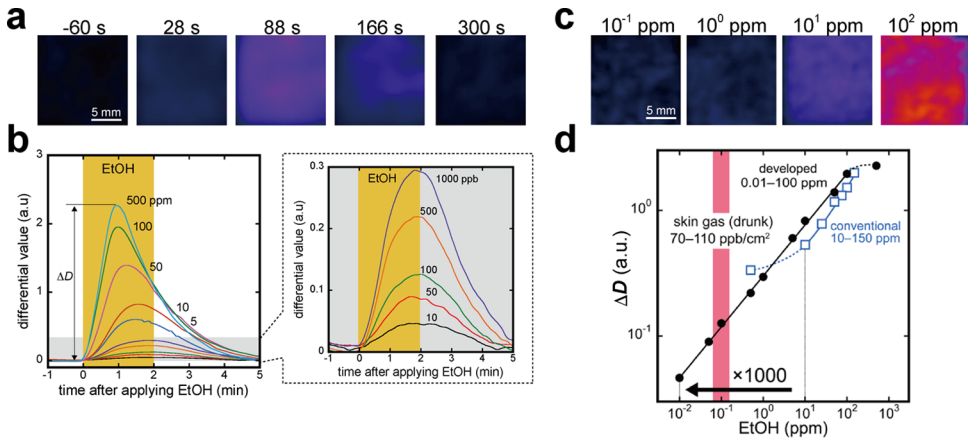

Figure 5. (a) Images of the changing fluorescence rate with the application of 500 ppm of gaseous EtOH. (b) Temporal change in the fluorescence rate with various concentrations of EtOH. (c) Images of the changing fluorescence rate that were obtained by the application of gaseous EtOH with various concentrations. (d) Comparison of the calibration curve and dynamic range between the previously developed system and the newly developed system.

became attenuated according to this distance. On the other hand, the 2D uniformity was the best (CV of 4.2%) when L was 60 mm. The intensity of the excitation light relatively decreased at the center of the excitation target when L was small. In contrast, when L was large, the excitation light intensity in the peripheral portion became smaller, causing the nonuniformity of the excitation light intensity (see Figure S5). Therefore, we fixed L at 60 mm for subsequent experiments.

Evaluation of a Gas Injection Device that Enables Two-Dimensional Gas Application. Figure 4a shows the fluorescence distribution and recovery rate of the gaseous EtOH concentration for representative results obtained in experiments using various gas diffusion membranes. Figure S6 shows pictures of the gas detection tubes after the measurement of the EtOH contained in the sample bag, and Table S2 shows the concentrations obtained from the detection tube. Figure 4b shows the temporal changes in the fluorescence intensity when 5 ppm of gaseous EtOH was applied to the ADH-immobilized mesh through various porous membranes. It was observed that when the applied gaseous sample was switched from dry air to gaseous EtOH, the fluorescence intensity gradually increased, and when switching back to dry air, a steady-state value is attained. It was found that even when using a developed gas application device that was designed to have a sealed space, the EtOH was appropriately replaced when the gaseous sample was switched. Also, the steady-state values and rate of the fluorescence intensity were found to change according to the pore diameter of the porous membrane; the same was found when using the gas detection tube. The steady-state value, ΔI, that was obtained by averaging the fluorescence intensity between 390 and 420 s after the start of the experiment and the slope of the fluorescence intensity from 180 to 240 s were calculated to evaluate the relationship between the pore size and the output signal (see Figure S7a,b). It was determined that the concentration of EtOH applied to the ADH-immobilized mesh was constant when the pore diameter was 5 μm or more. However, the logarithmic correlation between the pore diameter and the slope of ΔI or the fluorescence intensity ΔI was demonstrated for the case of a porous membrane with a pore diameter of 0.1−5 μm. This data supports the experimental data obtained from the gas detection tube. Although the concentration of EtOH that diffused via the porous membrane changed depending on the pore size, we can conclude that the concentration of EtOH does not decrease because of the gas diffusion membrane if the pore size was 5 μm or more. Figure 4c shows a comparison of the CV of the fluorescence distribution calculated from the fluorescence image of Figure 4a. The first data from the left of Figure 4a was obtained using the previous gas application method, and the fluorescence was concentrated at the center. Conversely, when using the gas application device in which the gas diffusion membrane was attached to the funnel-like flow-rate reducer, the distribution of the fluorescence over the entire mesh was observed. As shown in Figure 4c, the best uniformity of the fluorescence intensity was obtained using a poly(tetrafluoroethylene) (PTFE) membrane with a 5 μm pore diameter.

Quantitative Characteristics of the System. Figure 5a shows images of the changing rate of fluorescence when 500 ppm of gaseous EtOH was applied on the ADH-immobilized mesh via the 2D Mako using the new gas application device. Figure 5b displays the temporal change in the differential value with various concentrations of gaseous EtOH. The rate of fluorescence increased with the application of gaseous EtOH, and we observed that it recovered to its initial value after the application of gaseous EtOH ceased, as it was found in previous research. On the other hand, the changing rate of fluorescence showed a peak value before switching to the dry clean air with standard gaseous EtOH concentration over 5 ppm. It was determined that this was a result of the insufficient NAD^+ concentration required for the enzymatic reaction. However, NAD^+ concentration is sufficient for the transcutaneous gas that contains lower than 1 ppm EtOH concentration. Figure 5c displays images of the change in fluorescence rate when loading gaseous EtOH at various concentrations. The quantitative characteristics of the system were computed based on the peak value, ΔD, as shown in Figure 5d. The limit of quantification (LOQ) was 1.2 ppb, which was determined by substituting 10 times the background noise value into ΔD in the calibration equation (eq 1). This result indicates that the developed system had a sufficient dynamic range for the measurement of EtOH in transcutaneous gas.

$$\text{EtOH conc. (ppm)} = 0.303 \times \Delta D^{0.404} \quad (1)$$

DOI: 10.1021/acssensors.9b01658
ACS Sens. XXXX, XXX, XXX−XXX

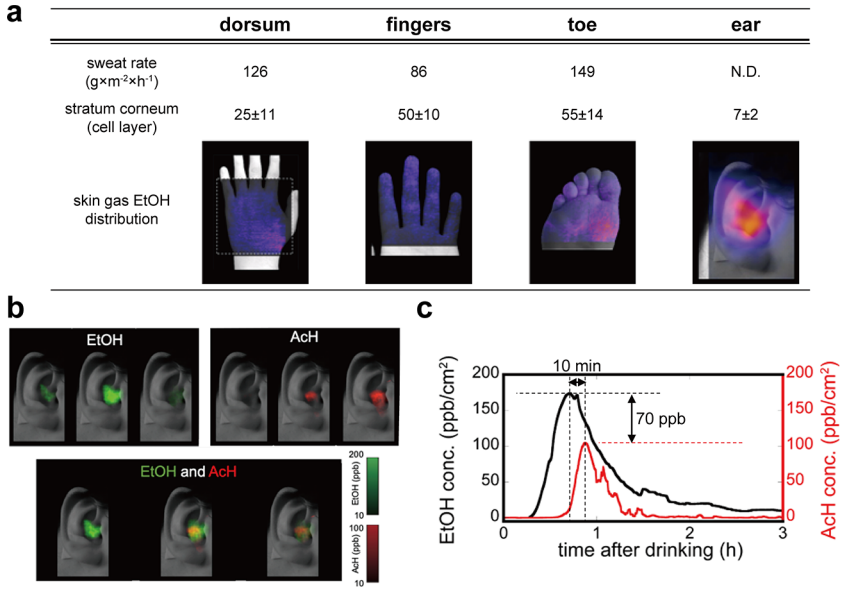

Figure 6. (a) Summary of the sweat rate, the number of stratum corneum layers, and transcutaneous EtOH concentration distribution for various body parts. (b) Concentration distribution of gaseous EtOH and AcH emitted from the ear after drinking alcohol, superimposed images of gaseous EtOH and AcH concentration distributions. (c) Temporal change of the transcutaneous EtOH and AcH concentrations emitted around the ear hole after drinking.

Furthermore, the selectivity of the sniff-cam is based on the substrate specificity of ADH. In the previous paper, we observed high selectivity of ADH against to EtOH among typical VOCs that were contained in exhaled breath and skin-gas after drinking.[22]

Spatiotemporal Imaging of Transcutaneous EtOH from Different Body Parts. First, we evaluated an irradiation power of the excitation light because UV light emitted from the system could cause skin damage. The experimental setup of the UV power assessment is shown in Figure S8. The power of UV light that was irradiated through the ADH-immobilized mesh and 2D Mako was decreased to 0.05% (0.0006 mW/cm^2) of original power (1.132 mW/cm^2). The UV light was absorbed and blocked by the ADH-immobilized mesh and the 2D Mako. A blocking power was comparable to a commercially available UV block filter (Table S3). However, long-time exposure to UV is possible to cause skin damage even though the irradiation power was weak. A minimal erythema dose (MED) is one of the values used to assess the effect of UV on skin.[30,31] The MED varied with skin color. We decided the maximum time of the experiment to be 4 h, which was the time for MED to be 0.5 for subjects of any skin color. Therefore, we considered that the effect of UV emitted from the sniff-cam on the skin is negligibly small.

Video S1 shows a spatiotemporal change of transcutaneous EtOH emitted around the palm region after drinking alcohol. As shown in the video, the spatiotemporal imaging of transcutaneous EtOH was made possible by the developed system. Emission of EtOH started about 2 min after drinking, then a high concentration of ethanol was observed about 30 min after drinking. The transcutaneous EtOH gas released from the palm fluctuated greatly with time at around 30 min after drinking. This fluctuation was considered to be due to palmar sweating, as described in a previous paper.[22] It is known that palms have a high density of eccrine sweat glands compared to other body parts, and mental sweating in addition to thermal sweating can occur. Transcutaneous gases are not only VOCs that are present in blood and released through the skin, but also VOCs are contained in sweat. However, it is not easy to monitor metabolism in the body using transcutaneous gases under the influence of perspiration.

We then decided to perform spatiotemporal imaging on various body parts to determine the optimal body part for metabolic monitoring of transcutaneous gas where the effect of perspiration is less, and the transmitted VOC concentration is high. Figure 6a summarizes the perspiration rate and the number of cell layers of stratum corneum,[18] and it shows the spatiotemporal images of EtOH levels obtained at the back of the hand, fingers, sole, and ear. This spatiotemporal information was not attainable with the conventional method of transcutaneous gas measurement as it is necessary to seal the target body part with a sample bag to collect VOCs via the skin. In contrast, it is possible to observe the distribution of transcutaneous gas in real-time and study the local dynamics of the specific body part using the newly developed system. For instance, a high concentration of EtOH was observed in the area around the ear. The stratum corneum around the ear is as thin as the eyelids, one of the thinnest skins of the human body. Besides, there are fewer sweat glands compared with the other body parts; hence, transcutaneous gas reflecting blood VOCs is likely to be emanated from the ear. Unlike the palms, these sites are not affected by sweating and would be a suitable site for the transcutaneous measurement of blood VOCs.

Spatiotemporal Imaging of EtOH and AcH Around the Ear. Spatiotemporal imaging of the EtOH and AcH was performed around the ear, where the transcutaneous measurement of blood VOCs using the developed system was deemed suitable. Note that the spatiotemporal imaging of AcH with the bio-fluorometric imaging method was based on the reverse reaction of ADH. In the previous work, we compare the reverse reaction of ADH and the forward reaction of ALDH to develop a biosensor that detects AcH.[28] As a result, the ADH-mediated biosensor showed a broader dynamic range with higher sensitivity compared to the ALDH-mediated biosensor.

DOI: 10.1021/acssensors.9b01658
ACS Sens. XXXX, XXX, XXX−XXX

Therefore, we have been utilizing the reverse reaction of ADH in the bio-sniffer[32] and sniff-cam[24] to detect AcH. Figure S9 shows a comparison of the quantitative characteristics of gaseous AcH concentration using the previous system and the newly developed system. The LOQ was improved by 10 times relative to the previous system, and it was possible to quantify 10 ppb of gaseous AcH. The dynamic range was 10 ppb to 3 ppm, which encompassed the concentration of transcutaneous AcH (43 ppb).[14]

Figure 6b shows the results of the spatiotemporal imaging of EtOH and AcH in the area around the ear, performed on the same subject on different days, as well as the results of the superimposed display of the data (see Video S2). Figure 6c shows the temporal changes in the EtOH and AcH concentrations calculated from the changing rate of fluorescence per 1 cm^2 in the vicinity of the ear canal. It was observed that the EtOH and AcH concentrations increased after drinking, reached a peak concentration, and then gradually decreased. This result indicates that metabolic monitoring can be realized by measuring the blood VOCs via transcutaneous gas in the area where the influence of perspiration is small, the skin is thin, and blood vessels are concentrated.

CONCLUSIONS

In this study, we developed a system aimed at establishing a new method that can investigate the release mechanism of transdermal VOCs in relation to local skin conditions. The developed system differs from the conventional measurement method in which it directly detects transcutaneous VOCs without the need for collecting procedures of the VOCs. It should also be noted that the sensitivity of this new system was comparable to that of methods using large analytical instruments such as GC−MS. The shapeshifting method using 2D Mako enabled accurate spatiotemporal imaging by equalizing the distance between the complex curved surface of the human body and the enzyme mesh. Transcutaneous gas has not been sufficiently studied because it is difficult to measure. However, it has been suggested that it is associated with skin diseases; therefore, the study of this gas is of importance. For example, Farkas et al. reported that EtOH and acetone concentrations in the skin might be associated with the exacerbation of psoriasis,[33] a common skin disorder.[34] In their review paper,[35] they described that, "It is expected that the development of methodologies measuring transdermal alcohol concentration will provide additional tools for clinicians to evaluate how alcohol influences skin physiology and different dermatological conditions including hyperproliferative diseases such as psoriasis" and "Different skin sites may show different ethanol levels depending on the thickness of the stratum corneum and on the density of follicles and sweat glands, thus leading to higher and lower concentrations, which may also have clinical relevance". We believe that the developed system and method can provide the required data for clinicians to investigate the conditions and that it may help to promote further research in the fields of metabolism and dermatology.

However, we demonstrated that it was possible to visualize the transcutaneous EtOH emanated from the human body only in the situation after drinking. In the previous paper, we showed the result of quantitative imaging of EtOH in exhaled breath without alcohol ingestion.[26] The concentration of breath EtOH without alcohol ingestion (around 0.1 ppm) was approximately 1000-times lower than after alcohol consumption (around 100 ppm). As same as in the exhaled breath, the concentration of transcutaneous EtOH without alcohol consumption is possible to be 1000-times lower than after drinking; therefore, the LOQ of the system must be better than 0.1 ppb. The LOQ of the current system was 1.2 ppb; thus, we have to improve over 10-times in the sensitivity of the system to visualize transcutaneous EtOH emanated from the subject without alcohol ingestion. However, the minimum limit concentration of standard gaseous EtOH that can be prepared is 10 ppb, and it is not possible to prepare the reliable standard gas with a ppt level concentration by the current method. Therefore, it is necessary to develop a low-concentration standard gas preparation method and improve the sensitivity of the system simultaneously.

In addition to the monitoring of metabolism by transcutaneous VOCs, we would also like to investigate the relationship between local lesions and transcutaneous VOCs.

ASSOCIATED CONTENT

Supporting Information

The Supporting Information is available free of charge at https://pubs.acs.org/doi/10.1021/acssensors.9b01658.

Effect of distance between skin and the ADH-immobilized mesh; experimental setup of excitation light uniformity; overview of gas application methods; dimensions and structures of the developed gas application device; characteristics of the porous membrane; distribution images of excitation intensity; images of gas detection tubes; transmitted EtOH concentrations; relationship between the pore size of the porous membrane and the sensor signal; experimental setup for UV light power; comparison of UV irradiation power under various conditions; comparison of the dynamic range for gaseous AcH quantification (PDF)

Spatiotemporal imaging of transcutaneous EtOH emitted from the palm skin after drinking (MP4)

Superimposed video of spatiotemporal changes of transdermal EtOH and AcH at around the ear (MP4)

AUTHOR INFORMATION

Corresponding Author

*E-mail: m.bdi@tmd.ac.jp. Tel: +81 3 5280 8091. Fax: +81 3 5280 8094.

ORCID

Kenta Iitani: 0000-0001-5608-8863

Kohji Mitsubayashi: 0000-0002-0709-4957

Notes

The authors declare no competing financial interest.

ACKNOWLEDGMENTS

This work was supported by the JSPS KAKENHI (Grant Numbers JP19J01649, JP17H01759, JP16J09604, and JP15H04013); the Japan Science and Technology Agency (JST); the Ministry of Education, Culture, Sports, Science and Technology (MEXT) Special Funds for "Cooperative Research Project of Research Center for Biomedical Engineering"; and Japan Insulin Dependent Diabetes Mellitus (IDDM) network. The authors would like to thank Uni-edit (https://uni-edit.net/) for editing and proofreading this manuscript.

DOI: 10.1021/acssensors.9b01658
ACS Sens. XXXX, XXX, XXX−XXX

REFERENCES

(1) Giannoukos, S.; Agapiou, A.; Brkić, B.; Taylor, S. Volatolomics: A Broad Area of Experimentation. *J. Chromatogr. B* **2019**, *1105*, 136−147.

(2) Phillips, M. Breath Tests in Medicine. *Sci. Am.* **1992**, *267*, 74−79.

(3) Buljubasic, F.; Buchbauer, G. The Scent of Human Diseases: A Review on Specific Volatile Organic Compounds as Diagnostic Biomarkers. *Flavour Fragrance J.* **2015**, *30*, 5−25.

(4) Broza, Y. Y.; Mochalski, P.; Ruzsanyi, V.; Amann, A.; Haick, H. Hybrid Volatolomics and Disease Detection. *Angew. Chem., Int. Ed.* **2015**, *54*, 11036−11048.

(5) Xu, M.; Tang, Z.; Duan, Y.; Liu, Y. GC-Based Techniques for Breath Analysis: Current Status, Challenges, and Prospects. *Crit. Rev. Anal. Chem.* **2016**, *46*, 291−304.

(6) Moeskops, B. W. M.; Steeghs, M. M. L.; van Swam, K.; Cristescu, S. M.; Scheepers, P. T. J.; Harren, F. J. M. Real-Time Trace Gas Sensing of Ethylene, Propanal and Acetaldehyde from Human Skin in Vivo. *Physiol. Meas.* **2006**, *27*, 1187−1196.

(7) Turner, C.; Parekh, B.; Walton, C.; Spanel, P.; Smith, D.; Evans, M. An Exploratory Comparative Study of Volatile Compounds in Exhaled Breath and Emitted by Skin Using Selected Ion Flow Tube Mass Spectrometry. *Rapid Commun. Mass Spectrom.* **2008**, *22*, 526−532.

(8) Mochalski, P.; King, J.; Unterkofler, K.; Hinterhuber, H.; Amann, A. Emission Rates of Selected Volatile Organic Compounds from Skin of Healthy Volunteers. *J. Chromatogr. B* **2014**, *959*, 62−70.

(9) Azzarelli, J. M.; Mirica, K. A.; Ravnsbæk, J. B.; Swager, T. M. Wireless Gas Detection with a Smartphone via Rf Communication. *Proc. Natl. Acad. Sci. U.S.A.* **2014**, *111*, 18162−18166.

(10) Neri, G. First Fifty Years of Chemoresistive Gas Sensors. *Chemosensors* **2015**, *3*, 1−20.

(11) Amann, A.; Costello, B. D. L.; Miekisch, W.; Schubert, J.; Buszewski, B.; Pleil, J.; Ratcliffe, N.; Risby, T. The Human Volatilome: Volatile Organic Compounds (VOCs) in Exhaled Breath, Skin Emanations, Urine, Feces and Saliva. *J. Breath Res.* **2014**, *8*, No. 034001.

(12) Khasag, N.; Sakiyama, S.; Toba, H.; Yoshida, M.; Nakagawa, Y.; Takizawa, H.; Kawakami, Y.; Kenzaki, K.; Ali, A. H. K.; Kondo, K.; Tangoku, A. Monitoring of Exhaled Carbon Monoxide and Carbon Dioxide during Lung Cancer Operation. *Eur. J. Cardiothorac. Surg.* **2014**, *45*, 531−536.

(13) Rubin, T.; von Haimberger, T.; Helmke, A.; Heyne, K. Quantitative Determination of Metabolization Dynamics by a Real-Time $^{13}CO_2$ Breath Test. *J. Breath Res.* **2011**, *5*, No. 027102.

(14) Mochalski, P.; Unterkofler, K.; Hinterhuber, H.; Amann, A. Monitoring of Selected Skin-Borne Volatile Markers of Entrapped Humans by Selective Reagent Ionization Time of Flight Mass Spectrometry in NO+ Mode. *Anal. Chem.* **2014**, *86*, 3915−3923.

(15) Yamada, Y.; Hiyama, S.; Toyooka, T.; Takeuchi, S.; Itabashi, K.; Okubo, T.; Tabata, H. Ultratrace Measurement of Acetone from Skin Using Zeolite: Toward Development of a Wearable Monitor of Fat Metabolism. *Anal. Chem.* **2015**, *87*, 7588−7594.

(16) Tsuda, T.; Ohkuwa, T.; Itoh, H. Findings of Skin Gases and Their Possibilities in Healthcare Monitoring. In *Gas Biology Research in Clinical Practice*; KARGER: Basel, 2011; pp 125−132.

(17) Naitoh, K.; Inai, Y.; Hirabayashi, T.; Tsuda, T. Direct Temperature-Controlled Trapping System and Its Use for the Gas Chromatographic Determination of Organic Vapor Released from Human Skin. *Anal. Chem.* **2000**, *72*, 2797−2801.

(18) Ya-Xian, Z.; Suetake, T.; Tagami, H. Number of Cell Layers of the Stratum Corneum in Normal Skin Relationship to the Anatomical Location an the Body, Age, Sex and Physical Parameters. *Arch. Dermatol. Res.* **1999**, *291*, 555−559.

(19) Wilke, K.; Martin, A.; Terstegen, L.; Biel, S. S. A Short History of Sweat Gland Biology. *Int. J. Cosmet. Sci.* **2007**, *29*, 169−179.

(20) Furukawa, S.; Sekine, Y.; Kimura, K.; Umezawa, K.; Asai, S.; Miyachi, H. Simultaneous and Multi-Point Measurement of Ammonia Emanating from Human Skin Surface for the Estimation of Whole Body Dermal Emission Rate. *J. Chromatogr. B* **2017**, *1053*, 60−64.

(21) Sekine, Y.; Toyooka, S.; Watts, S. F. Determination of Acetaldehyde and Acetone Emanating from Human Skin Using a Passive Flux Sampler—HPLC System. *J. Chromatogr. B* **2007**, *859*, 201−207.

(22) Arakawa, T.; Suzuki, T.; Tsujii, M.; Iitani, K.; Chien, P.-J.; Ye, M.; Toma, K.; Iwasaki, Y.; Mitsubayashi, K. Real-Time Monitoring of Skin Ethanol Gas by a High-Sensitivity Gas Phase Biosensor (Bio-Sniffer) for the Non-Invasive Evaluation of Volatile Blood Compounds. *Biosens. Bioelectron.* **2019**, *129*, 245−253.

(23) Arakawa, T.; Sato, T.; Iitani, K.; Toma, K.; Mitsubayashi, K. Fluorometric Biosniffer Camera "Sniff-Cam" for Direct Imaging of Gaseous Ethanol in Breath and Transdermal Vapor. *Anal. Chem.* **2017**, *89*, 4495−4501.

(24) Iitani, K.; Sato, T.; Naisierding, M.; Hayakawa, Y.; Toma, K.; Arakawa, T.; Mitsubayashi, K. Fluorometric Sniff-Cam (Gas-Imaging System) Utilizing Alcohol Dehydrogenase for Imaging Concentration Distribution of Acetaldehyde in Breath and Transdermal Vapor after Drinking. *Anal. Chem.* **2018**, *90*, 2678−2685.

(25) Rueden, C. T.; Schindelin, J.; Hiner, M. C.; DeZonia, B. E.; Walter, A. E.; Arena, E. T.; Eliceiri, K. W. ImageJ2: ImageJ for the next Generation of Scientific Image Data. *BMC Bioinformatics* **2017**, *18*, No. 529.

(26) Iitani, K.; Toma, K.; Arakawa, T.; Mitsubayashi, K. Ultra-sensitive Sniff-Cam for Biofluorometric-Imaging of Breath Ethanol Caused by Metabolism of Intestinal Flora. *Anal. Chem.* **2019**, *91*, 9458−9465.

(27) Murarnatsu, T.; Higuchi, S.; Shigernori, K.; Saito, M.; Sasao, M.; Harada, S.; Shigeta, Y.; Yamada, K.; Muraoka, H.; Takagi, S.; Maruyarna, K.; Kono, H. Ethanol Patch Test-A Simple and Sensitive Method for Identifying ALDH Phenotype. *Alcohol.: Clin. Exp. Res.* **1989**, *13*, 229−231.

(28) Iitani, K.; Chien, P.-J.; Suzuki, T.; Toma, K.; Arakawa, T.; Iwasaki, Y.; Mitsubayashi, K. Improved Sensitivity of Acetaldehyde Biosensor by Detecting ADH Reverse Reaction-Mediated NADH Fluoro-Quenching for Wine Evaluation. *ACS Sens.* **2017**, *2*, 940−946.

(29) Iitani, K.; Hayakawa, Y.; Toma, K.; Arakawa, T.; Mitsubayashi, K. Switchable Sniff-Cam (Gas-Imaging System) Based on Redox Reactions of Alcohol Dehydrogenase for Ethanol and Acetaldehyde in Exhaled Breath. *Talanta* **2019**, *197*, 249−256.

(30) Visscher, M. O. Skin Color and Pigmentation in Ethnic Skin. *Facial Plast. Surg. Clin. North Am.* **2017**, *25*, 119−125.

(31) Pathak, M. A.; Fanselow, D. L. Photobiology of Melanin Pigmentation: Dose/Response of Skin to Sunlight and Its Contents. *J. Am. Acad. Dermatol.* **1983**, *9*, 724−733.

(32) Iitani, K.; Chien, P.-J.; Suzuki, T.; Toma, K.; Arakawa, T.; Iwasaki, Y.; Mitsubayashi, K. Fiber-Optic Bio-Sniffer (Biochemical Gas Sensor) Using Reverse Reaction of Alcohol Dehydrogenase for Exhaled Acetaldehyde. *ACS Sens.* **2018**, *3*, 425−431.

(33) Farkas, Á.; Kemény, L.; Széll, M.; Dobozy, A.; Bata-Csörgo, Z. Ethanol and Acetone Stimulate the Proliferation of HaCaT Keratinocytes: The Possible Role of Alcohol in Exacerbating Psoriasis. *Arch. Dermatol. Res.* **2003**, *295*, 56−62.

(34) Al-Jefri, K.; Newbury-Birch, D.; Muirhead, C. R.; Gilvarry, E.; Araújo-Soares, V.; Reynolds, N. J.; Kaner, E.; Hampton, P. J. High Prevalence of Alcohol Use Disorders in Patients with Inflammatory Skin Diseases. *Br. J. Dermatol.* **2017**, *177*, 837−844.

(35) Farkas, Á.; Kemény, L. Psoriasis and Alcohol: Is Cutaneous Ethanol One of the Missing Links? *Br. J. Dermatol.* **2010**, *162*, 711−716.

DOI: 10.1021/acssensors.9b01658
ACS Sens. XXXX, XXX, XXX−XXX